Journal of Hydrology X 30 (2026) 100213

Contents lists available at ScienceDirect

Journal of Hydrology X

journal homepage: www.sciencedirect.com/journal/journal-of-hydrology-x

Letter

Global groundwater modeling: Proof-of-concept of 3D variably saturated flow simulation at kilometer resolution

Stefan Kollet [a,b,*], Alexandre Belleflamme [a,b], Laura Condon [c], Muhammad Fahad [a], Klaus Goergen [a,b], Reed Maxwell [d], Bibi Naz [a,b]

[a] Institute of Bio- and Geosciences, Agrosphere (IBG-3), Forschungszentrum Jülich GmbH, Jülich, Germany
[b] Center for High-Peformance Scientific Computing in Terrestrial Systems, Geoverbund ABC/J, Germany
[c] Department of Hydrology and Atmospheric Sciences, University of Arizona, Tucson, USA
[d] Department of Civil and Environmental Engineering, Princeton University, Princeton, USA

ARTICLE INFO

Editor: Hoori Ajami

ABSTRACT

The proof-of-concept study presents, for the first time, the results of integrated numerical hydrological simulations at kilometer resolution on a global scale. Using available datasets and applying significant simplifications to the real terrestrial system, the model was informed with hydrofacies, soil texture and topographic slopes, and effective recharge at the upper boundary. A steady-state spin-up was performed, resulting in a 3D pressure head distribution of the water continuum from 60 m deep variably saturated groundwater to surface water. Relative saturation and diagnostic water table depth were examined, resolving variability over several orders of magnitude. In our opinion, the added value of the partial differential equation (PDE) based simulations outweighs the computational resources required, which are considerable. These simulations are possible, because of the advent of massively parallel, accelerator based supercomputer architectures and performance portable scientific software. While the current simulation results may not be reliable from the perspective of stakeholders at this stage of model development, the study demonstrates the feasibility of prognostic groundwater simulation at the global scale, and will stimulate future model improvements, including the quantification of uncertainties. Simultaneously, the study opens new avenues for future research in the context of hyper-resolution global Earth system modelling.

1. Main

1.1. Background

The term Global Water Modeling (GWM) is being coined in the hydrologic and land surface modeling communities encompassing global models simulating the water cycle on the continent. GWMs parameterize the water cycle at and below the land surface in different ways, also connecting to the energy and biogeochemical cycles and human interventions (Telteu et al., 2021). GWMs are generally applied in offline mode, that is they are driven by atmospheric forcing without two-way coupling with an atmospheric model. This, and simplifications with respect to groundwater flow and interactions with the vadose zone and surface water, means that dynamic closure of the water cycle is often not considered. With such simplifications, the water continuum is essentially split up into the different compartments and then again coupled, often via an operator splitting approach (Kavetski and Clark, 2011). Compartmentalization, however is problematic, because previous studies showed that non-linear feedbacks in the water continuum are important and need to be included in an accurate representation of hillslope processes across scales (Clark et al., 2015; Condon et al., 2021; Fan et al., 2019).

The origin and conceptual starting point of GWMs is diverse, but perhaps can be put into three major strands, modified from (Fisher and Koven, 2020). In the first strand, while GWMs run offline, many of these models can be traced back to climate models, which led the early development at the global scale and also at the regional (continental) scale due to the need for land surface boundary conditions for atmospheric simulations. To solve the boundary value problem, these GWMs focused originally on the connection of the terrestrial energy and water balance mainly via evaporation and transpiration, and the basic partitioning of precipitation (rain, snow, ice) on the land surface into storage,

* Corresponding author at: Institute of Bio- and Geosciences Agrosphere (IBG-3), Forschungszentrum Jülich GmbH, Jülich, Germany.
E-mail address: s.kollet@fz-juelich.de (S. Kollet).

https://doi.org/10.1016/j.hydroa.2025.100213
Received 28 March 2025; Received in revised form 10 December 2025; Accepted 14 December 2025
Available online 18 December 2025

infiltration and runoff. Examples include CLM (Lawrence et al., 2019), Noah-MP (Niu et al., 2011), and Orchidee (Krinner et al., 2005). The second strand includes hydrologic models (conceptual, distributed, physics based, parsimonious), which focused the closure of the water balance with bulk energy parameterizations of evapotranspiration (e.g., Penman) and precipitation as sink and source terms, respectively. Examples include mHM (Samaniego et al., 2010), HBV (Lindström et al., 1997), and LISFLOOD (Knijff et al., 2010). In the third strand, GWMs focused on human water usages using allocations and storage-release parameterizations of the bucket type in conjunction with statistical, economic information. Examples include WaterGAP (Müller Schmied et al., 2021) and PCR-GLOBWB (Sutanudjaja et al., 2018). In recent years, the overlap of the different strands has been increasing considerably pushing towards a unifying Earth System Modeling (ESM) approach including prognostic modeling of *all* natural processes across relevant space and time scales including two-way feedbacks and human interventions (Pan et al., 2025).

GWMs have an intuitive appeal reflected in studies that have been published in high-impact international scientific journals and (social) media (De Graaf et al., 2015; Fan et al., 2013; Reinecke et al., 2019; Verkaik et al., 2024). In our opinion, the appeal stems from information on the global water cycle *everywhere* that is consistent internal to the model. This information is usually not available in space and time. However, there has been anecdotal and documented (Gnann et al., 2023) resentments towards GWM results for multiple reasons. One of the most prominent reasons is uncertainty in the simulation results, which has not been adequately taken into account. Sources of uncertainty include, e.g., conceptual and mathematical model formulation at scale, as well as data uncertainty and scarcity for model setup and evaluation alike. For example, De Graaf et al. (2019) show results at roughly 10 km lateral spatial resolution on environmental flow limits influenced by groundwater abstraction, where hydraulic head differences on the order of 10^{-2} to 10^{-1} m are relevant. They conclude that by 2050, environmental flow limits will be reached for some 42 to 79 per cent of the global watersheds. This accuracy in head difference and flow limit calculations is in stark contrast to uncertainties in depth to groundwater estimates recently presented by Reinecke et al. (2024), which are on the order of 10^{-2} to 10^{-1} m. Thus, before policy relevant results can be communicated, more work is required to improve the representation of groundwater and interactions with surface water in large scale models.

Another major reason for continuing skepticism from the hydrogeologic community (Andréassian, 2023; Gleeson et al., 2021) towards GWMs is the local to regional nature of groundwater and also surface water flow systems. There is no global groundwater-surface water circulation. The largest relevant spatial scale is the continental watershed and aquifer scale. Below that scale, water systems are commonly treated individually reflected also in conceptual model construction based, e.g., on the Hydrologic Unit Codes (HUCs) (Hydrologic unit maps, 1987). Ultimately, however, global scale connections of the water cycle are made through atmospheric circulations. Conversely, groundwater-surface water interactions are often oversimplified in GWMs, with groundwater frequently omitted or only weakly coupled to subsurface flow and surface water, effectively fragmenting the water continuum. Thus, the impression persists that GWMs ultimately deal with local to regional water processes, which they are not able to address adequately because of the lack of physical process representation and missing local information.

The current lack of physics-based, prognostic modeling of groundwater surface water flow and, in GWMs, the usual compartmentalization into saturated zone (often termed groundwater), unsaturated zone, and surface water has thereby far-reaching consequences. While the contributions of groundwater to the global water cycle appear to be indirect and local, they are of major importance. Groundwater sustains evapotranspiration and closes the continental water balances from source (e.g., mountains) to sink (oceans) areas everywhere. In fact, groundwater maintains continental discharge via baseflow and, through many feedbacks and interactions, keeps the continents in a delicate, life sustaining dynamic water equilibrium (Famiglietti, 2014; Sophocleous, 2002). This equilibrium is coming under pressure and is shifting due to global change at different space and time scales in an unknown fashion. Since the continents constitute a sink to atmospheric water (Keune et al., 2018), where precipitation (P) exceeds evapotranspiration (ET), P-ET $>$ 0, the moisture state, in fact the chemical potential, of the continents will influence the continental water sink and, thus, the continental water balance, and potentially also meso- and global scale atmospheric circulations. Thus, after all, variably saturated groundwater flow and interactions with surface water and land surface happen in a non-linear continuum, they are relevant from the local to the global scale and potentially also for global moisture redistribution (Yang et al., 2025).

Thus, variably saturated subsurface water, groundwater, and surface water needs to be included in large-scale ESMs as a nonlinear continuum in order to have prognostic modeling capabilities from bedrock to the top-of-the atmosphere. Currently, there is a push for seamless (weather to climate) simulations on the order of km-scale spatial resolution (Bauer et al., 2021; Stevens et al., 2024), which also considerably alters the physics representation in the models (Prein et al., 2015). The expectation is that major prognostic biases related to, e.g., global temperature and precipitation distributions, including extremes, can be resolved this way at the climate time scale (Stevens et al., 2024). At this resolution, individual river corridors become visible in, e.g., remote sensing data, however, not in ESMs, because groundwater convergence and baseflow is not simulated. Coupling ESMs with the aforementioned GWMs is not an option either, because they do not provide groundwater modeling capacities in a continuum approach across the variably saturated soil zone and an integration with surface flow. Here, physics-based Integrated Hydrologic Models (IHMs), where 2D/3D surface and subsurface hydrodynamics are treated in continuum approach are an alternative (Brookfield et al., 2023; Clark et al., 2017).

IHMs are Partial Differential Equation (PDE)-based and numerically implement a combination of conservation and movement equations. The mathematical problem is closed via boundary and initial conditions and solved numerically on a grid. IHMs need information on hydraulic parameters at the grid level, which introduces uncertainty because of heterogeneity at the subgrid scale and data scarcity. In this study, we present a 3D continuum approach for groundwater-surface water flow modeling at km-scale resolution using the IHM ParFlow (PF) (Kuffour et al., 2020 for an overview), which lends itself for an implementation in ESMs, as has been demonstrated in regional climate simulations (Furusho-Percot et al., 2019; Poshyvailo-Strube et al., 2024) and is currently scaled up to the globe. Results from proof-of-concept simulations are provided that show the potential for consistent prognostic groundwater-surface water flow modeling everywhere, i.e., globally, at high resolution, following the motivation by (Bierkens et al., 2015; Wood et al., 2011). The role of compute resources and different sources of uncertainty are discussed including the steps forward for implementing prognostic water models into ESMs.

1.2. Terminology and approach

In this study, we simulate variably saturated groundwater flow in the subsurface at the global scale in a proof-of-concept approach. We refer to variably saturated groundwater flow as the movement of water in the porous medium of the subsurface. Thus, we do *not* distinguish between the unsaturated or vadose zone (also often referred to as the soil zone) and the saturated zone and mathematically treat groundwater flow with a combination of a continuity and movement equation (Darcy's law) that can also include confined and unconfined aquifers. In fact, such integrated hydrologic models do not exhibit strong structural differences amongst each other, which has been shown in intercomparison studies (Kollet et al., 2017; Maxwell et al., 2014).

The key challenge of groundwater flow modeling is the

representation of subsurface heterogeneity. In the groundwater flow modeling, the heterogeneity of the subsurface is expressed via the spatial distribution of so-called hydrofacies. The definition of the term hydrofacies has been established in the groundwater flow and transport community and refers to a "homogeneous sedimentological unit or a homogeneous but not necessarily isotropic hydrogeological unit (Anderson, 1989), formed under characteristic conditions, which lead to characteristic hydraulic properties" (Klingbeil et al., 1999). In groundwater flow modeling, the hydrofacies distribution in space can be delineated based on geologic knowledge, maps, models of the subsurface, and geostatistical methods, which are used to apply knowledge on the spatial structure and continuity of geologic units often derived from geologic and sedimentologic data. In many cases, the model of spatial hydrofacies distribution can be conditioned on observations from boreholes (e.g., drilling logs) and geophysical surveys. While complex (un-)confined aquifer architectures and tectonic structures across spatial scales pose a major challenge, because they are difficult to characterize in the field and to represent in hydrofacies models over large regions, they can be efficiently implemented in IHMs (Tijerina-Kreuzer et al., 2024). This study constitutes a first step and does not take into account these structures, in addition to Karst and permafrost systems. Therefore, the simulation results (shown below) for these regions must be treated with caution.

For groundwater flow modeling, the hydrofacies distribution is translated into hydraulic properties by applying hydraulic knowledge on the associated lithofacies (hard rock, soft rock, soil) from literature or hydraulic and hydrogeophysical testing. If the hydrofacies information is derived from soil maps, pedotransfer functions are used in the translation.

We applied the variably saturated groundwater-surface water flow code ParFlow (Jones and Woodward, 2001; Kollet and Maxwell, 2006; Maxwell, 2013). In ParFlow, flow in the porous medium of the subsurface is treated as a continuum using the 3D mixed-form of Richards equation, which is valid everywhere under the assumption of, e.g., an infinitely mobile air phase and equilibrium of pressure and saturation. This means that, e.g., a free water table and its nonlinear movement and interactions with partially saturated porous media above toward the land surface are implicit in the governing equation. Because ParFlow's solution is expressed in pressure (and saturation), diagnostic variables such as water table depth and groundwater recharge in transient simulations must be estimated in a postprocessing step (or online during the simulation).

Because ParFlow applies a free surface overland flow boundary condition to close the mathematical problem of variably saturated groundwater flow, surface water flow is intrinsically part of the solution. Thus, processes representation includes, e.g., the intersection of (perched) groundwater with the land surface (excess saturation) and resulting overland flow, and Hortonian runoff (excess infiltration). Discharge at every grid point of surface water ponding at the surface can be calculated using the Saint Venant equation with the kinematic wave approximation. Again, key non-linear processes are simulated this way avoiding coupling of different models and linearization via, e.g., operator splitting. Illustrative examples are provided in Kollet and Maxwell (2006), refer to (Kuffour et al., 2020) for an overview.

The boundary value problem is implemented on a structured grid using a finite difference/control volume discretization approach, in this study's setup with a constant discretization of 1 km in the $x-$ and $y-$ directions and variable discretization in the z-direction down to 60 m depth. The number of grid cells in the $x-, y-, z$-direction is 43200, 17400, and 15, respectively, resulting in a total of $1.1x10^{10}$ grid cells. Note, this includes the ocean areas (see Methods). The resulting system of equations is solved using advanced solver and preconditioner technologies based on Newton-Krylov and multigrid approaches, respectively. ParFlow has been implemented from the single column scale to continental scale. Here, we present the first application of ParFlow at the global scale, and the first application of a continuum model of 3D variably saturated groundwater surface water flow at the global scale.

The global model was constructed based on the workflow by Bellefflamme et al. (2023) for generating ParFlow input data. The workflow is efficient, transferable to any region/watershed in the world and publically available. The input data consists of topographic slopes, and hydrofacies information, which is transferred to hydraulic parameters and values via an indicator approach. The indicators are integers distributed in 3D over the computational grid, each indicator representing an individual hydrofacies (Fig. 1).

The construction of the 3D hydrofacies distribution in the ParFlow IHM is based on SoilGrids v2017 (Hengl et al., 2017) and below the depth-to-bedrock variable of SoilGrids soil hydraulic are used from the Gleeson et al. (2014) GLHYMPS subsurface dataset based on global lithology maps. In addition to Fig. 1, which illustrates the distribution of ParFlow hydrofacies from the GLHYMPS dataset, Fig. 5 shows areas of the global model domain with permafrost, glaciated regions (e.g. mountain glaciers and ice sheets), and karst and karstic systems with complex physics leading to highly heterogeneous permeability distributions including non-Darcian flow phenomena. Note that these map layers (Methods section) are also plotted on Fig. 3 and Fig. 4 to indicate simulation results, which may be considered less reliable or unreliable.

In the spinup simulation, at the land surface, the model was forced with climatologic monthly mean values of effective recharge that is the difference between precipitation and evaporation, $R_{eff} = P - ET$ (Fig. 2). While surface water is included in the continuum via the overland flow boundary condition allowing water to pond with a free surface due to e.g. exfiltration along river corridors, lateral routing is not performed in order to simplify the Jacoby matrix. Instead, excess water is removed to accelerate the initial spinup phase. When excess water is removed and the dynamic equilibrium is approached, lateral overland flow is activated including reinfiltration based on the approach of Kollet and Maxwell (2006).

In Methods, more details are provided on the generation of the hydrofacies and indicator distribution, hydrologic consistent topographic slopes, monthly effective infiltration fields, and implementation of boundary conditions.

To efficiently perform global 1 km-resolution continuum simulations of a highly-nonlinear physical problem, i.e. variably saturated groundwater surface water flow, massively parallel software is required beyond the state-of-the-art MPI distributed memory parallelism. ParFlow has been built from the ground up for massively parallel High Performance Computing (HPC) environments, which has been demonstrated in a number of studies (Burstedde et al., 2018). Going beyond the state-of-the-art of current integrated hydrologic modeling tools, ParFlow has been made performance portable (Hokkanen et al., 2021). In the development an existing macro based code interface in ParFlow has been exploited in order to abstract the parallelism and also memory management from the domain specific scientist in a performance portability layer. This layer serves as a front end to the domain scientist programming in ParFlow. As backends, via the portability layer, ParFlow supports well-known distributed memory parallelism with MPI, OpenMP parallelism, and accelerator parallelism with CUDA and a Kokkos, which also supports AMD GPUs. The accelerator backends can also be combined with MPI for efficient heterogeneous computing on the most modern HPC systems. In more idealized scaling experiments, ParFlow shows excellent performance on the order of 10^3 GPUs (Hokkanen et al., 2021), which affords the type of large scale simulations presented here. Here, we applied the MPI-CUDA backend in the HPC environment JUWELS of the Jülich Supercomputing Centre, Germany (Alvarez, 2021). JUWELS consists of different modules, where the so-called Booster module was used in the simulations. The Booster encompasses 936 compute nodes (2 x AMD EPYC Rome with 2 x 24 cores, 512 GB RAM), each connected to 4 GPUs. The interconnect is Infiniband HDR. We utilized a total of 80 nodes and 320 GPUs in the simulations. This resulted in an optimal loading of the GPUs following different trials

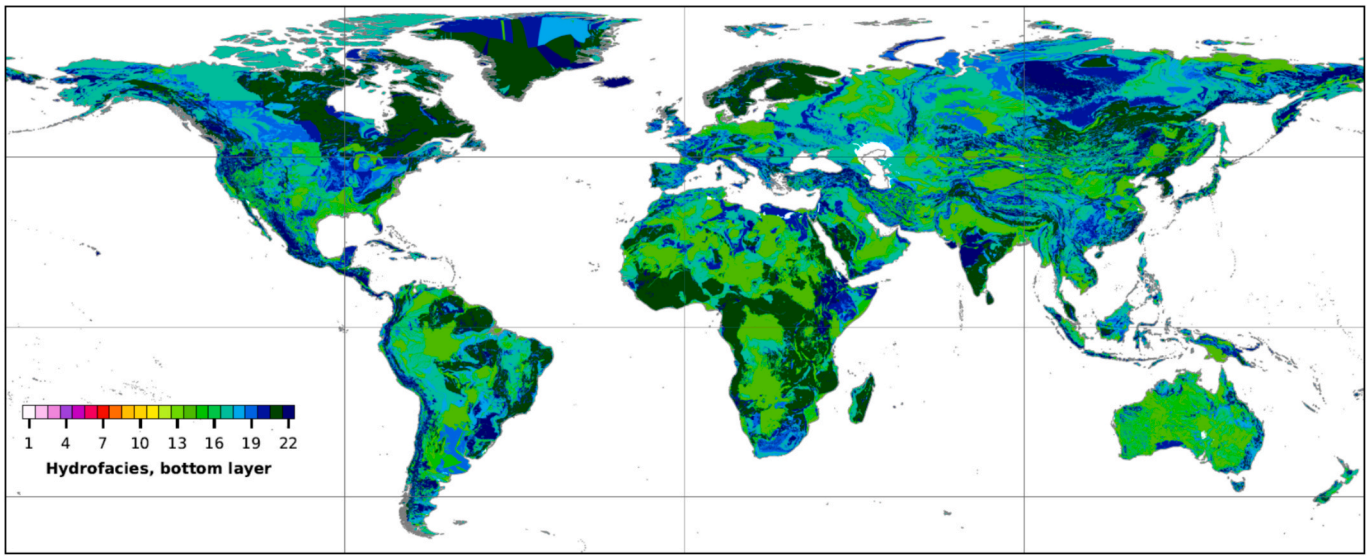

Fig. 1. ParFlow integer indicator distribution of the applied hydrofacies distribution in one model layer.

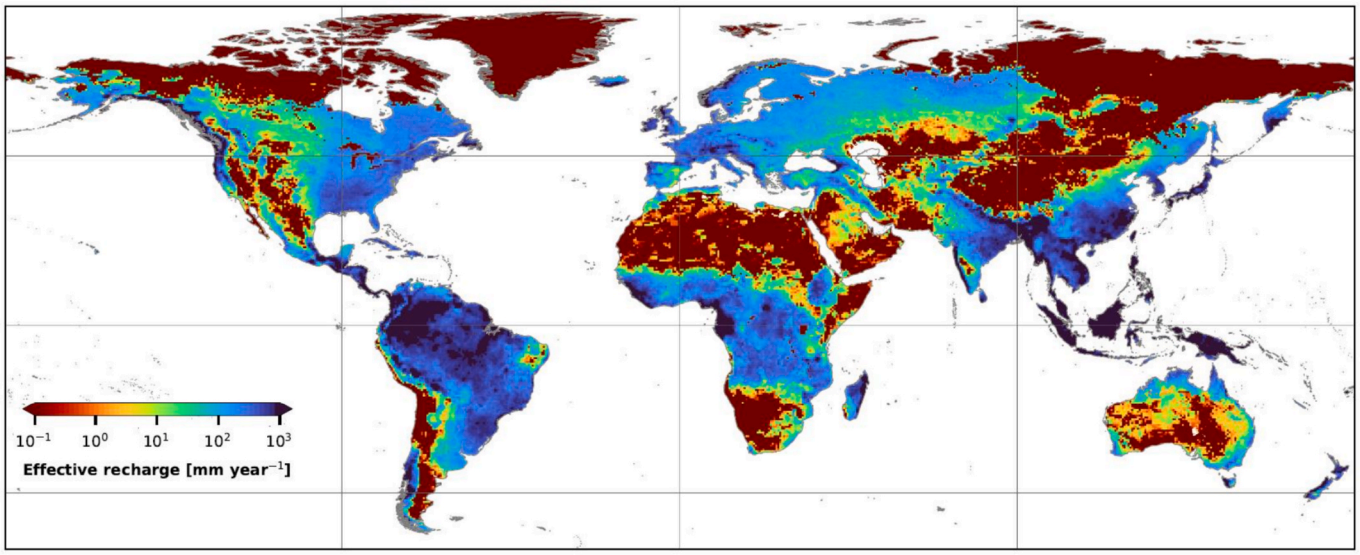

Fig. 2. Decadal average distribution of effective recharge $R_{eff} = P - ET$ [mm/year].

and a runtime of less than two hours wall-clock per simulated month near the completion of the spinup, when especially the number of non-linear iterations has decreased considerably.

In our proof-of-concept study, the spinup was performed by repeatedly forcing ParFlow with the global climatologic mean (P-ET) data set until a dynamic equilibrium was achieved (Methods section). This was checked by comparing pressure head distributions at the beginning and end of the simulated year and evaluating the temporal evolution of global and regional total storage. The result is a steady state image of global 1 km resolution pressure head distributions, which is in dynamical equilibrium with the R_{eff} forcing. The pressure head values can be used to calculate different diagnostic variables such as water table depth, saturation, water storages, etc. Note, while at this stage of the spinup process regional and local steady-state convergence has not been obtained everywhere, the simulation results are useful in showing the feasibility of kilometer-scale simulations and act as proof-of-concept at the global scale. The robustness with respect to hydraulic head, relative saturation and diagnostic variables such as groundwater table location and stream discharge will be evaluated in ensuing studies.

2. Results and discussion

The steady state simulation resulted in spatial patterns in soil moisture and pressure head, which reflect the physically-based 3D variably saturated flow determined by the 3D hydrofacies distribution, topography and R_{eff} forcing at the top (Fig. 2). Groundwater convergence happens along the river corridors resulting in continental drainage sustained by baseflow to lower and higher order streams. Note, rivers are not prescribed in the simulations but evolve from 3D groundwater flow, physically-based on the topographic representation in the model. From the simulation results *all* hydrologic variables of interest can be derived for the subsurface, because the full 3D pressure head distribution is available everywhere. For example, in Fig. 4 groundwater table depth was estimated from the vertical pressure head distribution at each individual pixel. While spinup is not complete regionally, it appears that generally shallower water tables are simulated in comparison to other global water models (Reinecke et al., 2024).

At 1 km resolution, hydrologic variables and variances are resolved over more than three orders of magnitude, which affords unprecedented

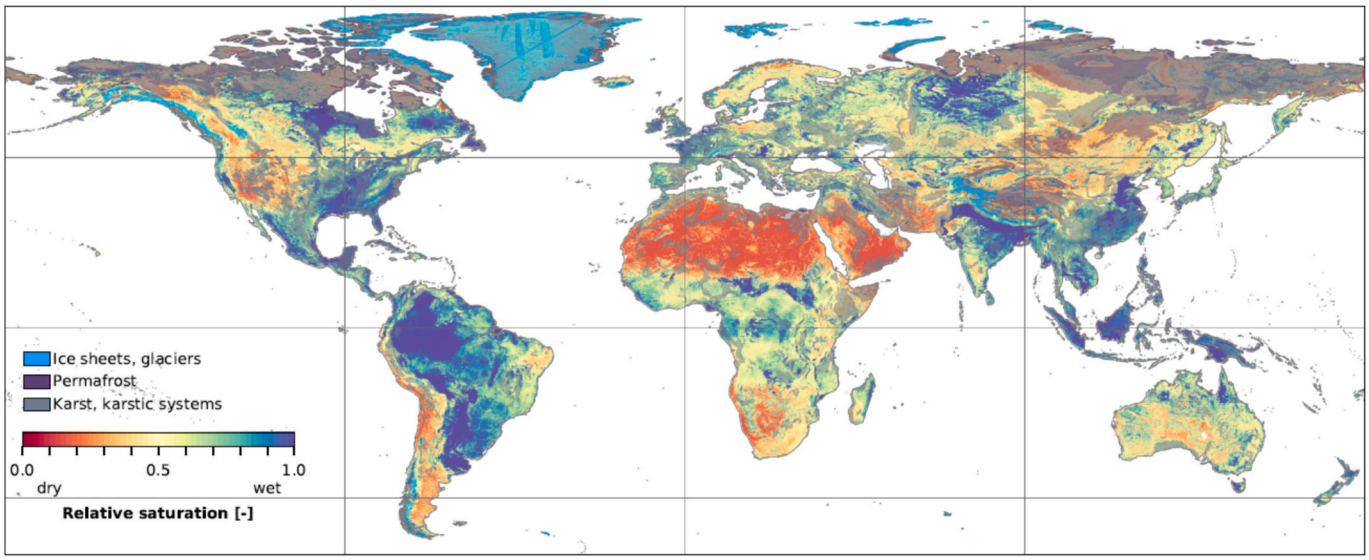

Fig. 3. Global distribution of simulated relative saturation in the top model layer (top 2 cm).

scaling analyses at the global scale. Fig. 4 shows water table depth globally and at an intermediate zoom level over parts of the southern hemisphere showing resolved river corridors from order six to one streams produced by 3D groundwater convergence along river corridors. Clearly, water table depth and relative saturation are inversely correlated, which is intuitive since shallow groundwater leads to moister conditions at near the land surface. The strength of this correlation depends on the local hydraulic properties and vertical hydrogeologic heterogeneity.

In the spinup simulations, the spatial distribution of the hydrologic variables depends mainly on the 3D hydrofacies distribution and 2D distribution of R_{eff}. In fact, the groundwater table distribution is mainly determined by the ratio of R_{eff} with some effective hydraulic conductivity. Therefore, the representation of hydrogeologic heterogeneity and hydrologic forcing at the land surface is key. Figs. 3 and 4, thus, exhibit a number of artifacts that are a direct result of the quality and resolution of the input information with respect to soil, hydrogeology and R_{eff}. For example, there are stripe-like and checkerboard patterns in the Arctic and regions in a.g. North America around the Great Lakes, respectively. Note, however, that karst and karstic systems, glaciated, and permafrost regions, such as the Arctic, are generally not simulated with the appropriate physics. Therefore, for transparency, we overlaid the simulation results in Figs. 3 and 4 with a unified map of glaciated and permafrost regions, and karst and karstic rocks. The map overlay based on Fig. 5 (Methods section) shows that variably saturated groundwater flow is an inherently complex, multi-physics problem, which will require considerable model development in future.

In hydrogeology, there will arguably never be enough data to inform a global hydrogeologic model at hyperresolution in 3D including tectonic structures and fault systems in the deep and the shallow subsurface. The same can be said for validation data especially *in-situ* water table depth and piezometric head observations. While there are data sets with good temporal and spatial coverage, large regions remain data-free or data-poor, which is not expected to change in future (Jasechko et al., 2024). Remote sensing information in combination with groundwater flow models, *in-situ* observations and artificial intelligence (AI) technologies will help in filling data gaps and generating time series of images at the global scale (Adams et al., 2022; Ibrahim et al., 2024). In these approaches, results from 3D physics based models, as presented in this study, will play a major role in training various machine learning/deep learning (ML/DL) models.

This study constitutes the advent of hyperresolution 3D prognostic, PDE-based groundwater modeling at the global scale solving variably saturated groundwater and surface water in a continuum approach, i.e., with one set of equations without compartmentalization of the saturated and vadose zone and surface flow. Additional model physics will be needed to simulate e.g. permafrost and karst regions appropriately. This physics-based approach comes at the expense of long compute times and large input and output data sets. The simulations were performed on 80 compute nodes of the JUWELS (JUlich Wizard for European Leadership Science) high-performance computing system of the Juelich Supercomputing Centre, Juelich, Germany. On each compute node, four CPUs each connected to one NVIDIA A100 GPU was used resulting in a total of 320 GPUs to perform the simulations efficiently. This was made possible by advancing ParFlow into a performance portable, exascale-ready scientific software (Hokkanen et al., 2021). Efficient application of the compute resources achieved one year simulation time in about 1.5 days wall-clock time given the climatologic R_{eff} forcing and hydrofacies distribution.

The question remains whether the added value of hyperresolution prognostic PDE-based groundwater-surface water modeling at the global scale is commensurate with the large computational and associated energy expense. Clearly, prognostic modelling is not warranted in all cases. While cases depend on the questions that need to be answered, some general rationale can be made for physics based modeling. For example, we argue that if a pure forecasting task needs to be solved and observational data is available for training or calibration, parameterized models may suffice. This is especially valid for regional studies that deal with very applied and engineering challenges. This is less so at the large scale, where most regions are ungauged. This is especially true in the comparison of the Global North and South. Thus, in the intermediate future, prognostic groundwater-surface modeling may contribute to information equity similar to global atmospheric reanalysis products. In our opinion, global scale modeling is less about solving pure forecasting tasks, which are mainly confined to local aspects of water resources planning etc. Global prognostic models provide a physics based image of the state and fluxes of the subsurface that is consistent everywhere similar to global atmospheric models applied in climate studies. Our expectation is that we can gain general understanding and, thus, achieve transferability of findings that are supported by universally valid physical principles. In addition, we are interested in closure of the water and also energy cycles from groundwater across the land surface to the top of atmosphere by coupling to land surface and atmospheric models. In other words, we want to inject groundwater into Earth system models for feedback simulations similar to previous studies at the continental or regional climate modeling scale (Furusho-Percot et al., 2019;

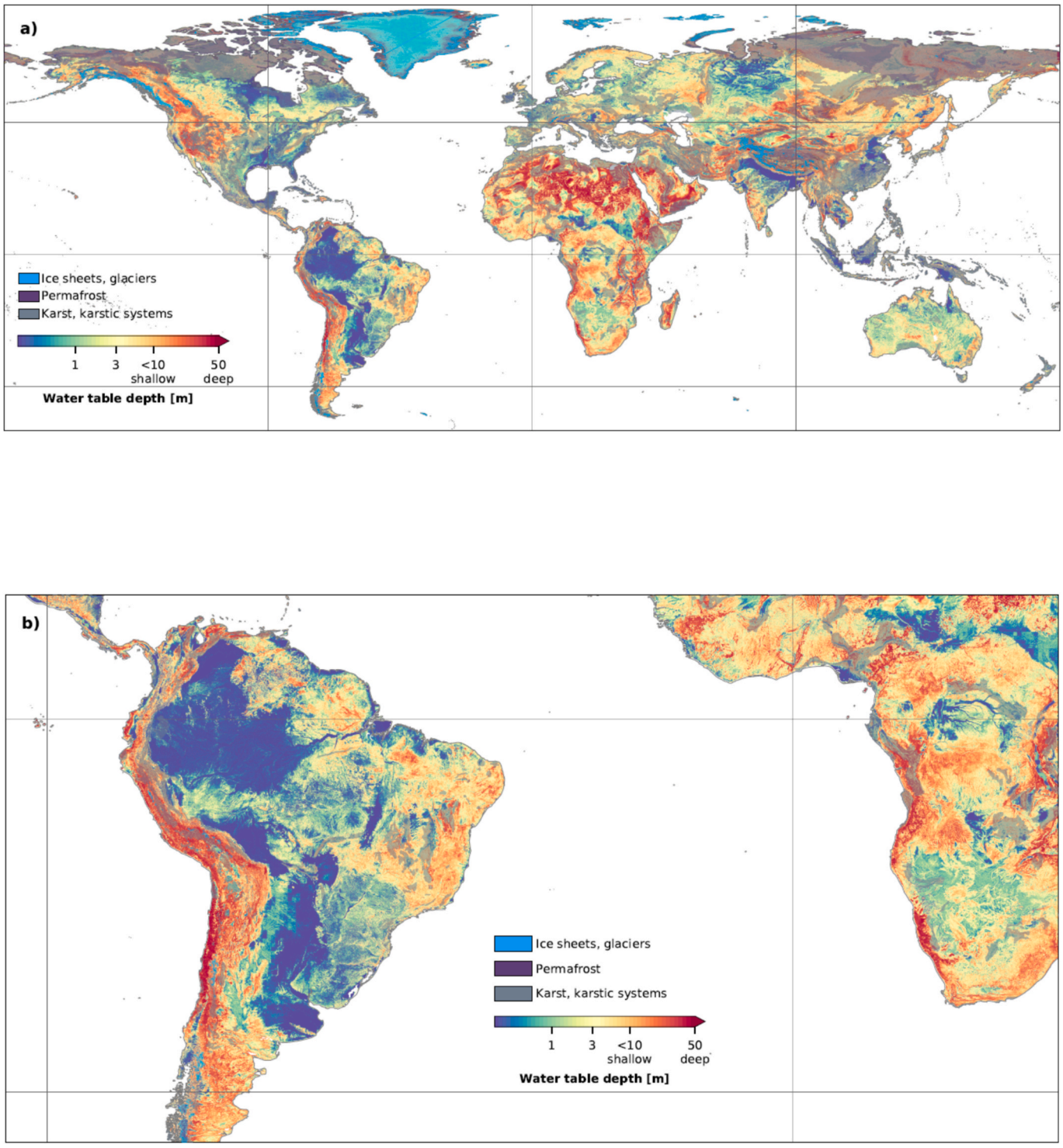

Fig. 4. a) Global distribution of groundwater table depth calculated from the vertical pressure head distribution at each individual pixel; b) zoom over parts of the southern hemisphere.

Poshyvailo-Strube et al., 2024; Yang et al., 2023). Applying physics-based variably saturated groundwater flow models such as ParFlow allows testing of simplifying assumptions related to e.g. hydrogeologic complexity and 3D flow representation, which can not be done with existing approaches in ESMs. These models will be extremely useful in climate studies, story line simulations and counterfactuals, including human interventions and transferability of the results. Ultimately, global, prognostic model based data sets will be available, which are continuous in space and time for training large scale machine learning and deep learning models, something that is common place in the atmospheric domain, yet prominently missing in the groundwater domain at the global scale, because of lack of prognostic modelling approaches.

In global scale models, assessing uncertainty due to large data gaps with respect to the hydrofacies distribution, large scale tectonics and in-situ and remotely sensed observations will remain one of the largest challenges in future. Uncertainty analyses with respect to, e.g., hydrofacies distribution often require simulations of multiple realizations. Done right, each realization would require a full spinup toward dynamic

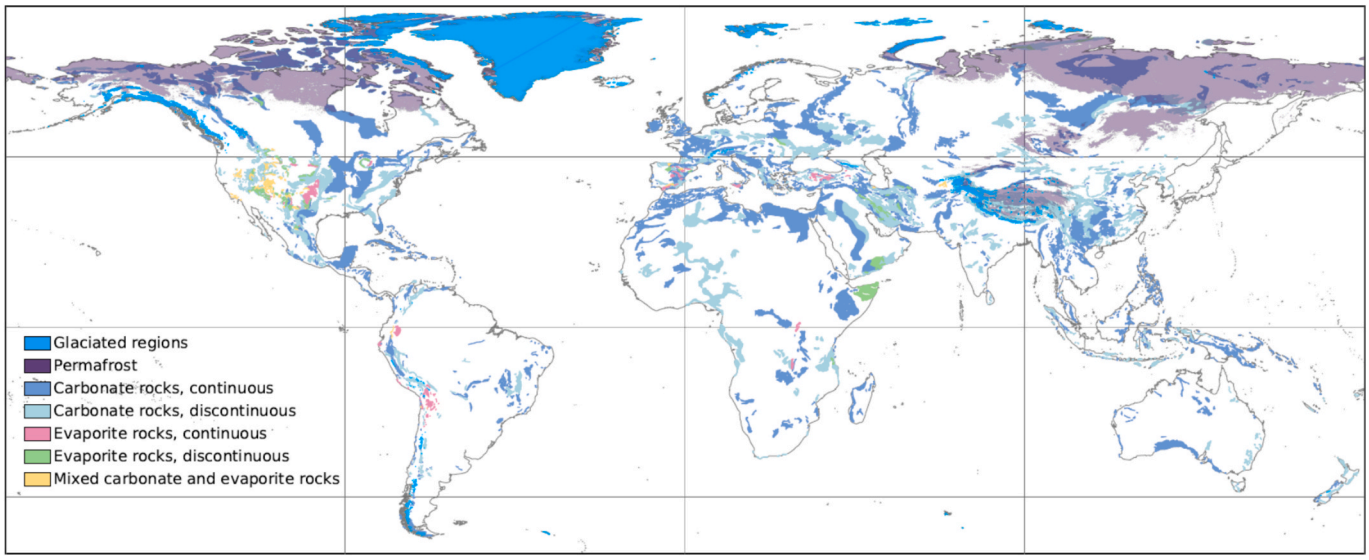

Fig. 5. Global distribution of glaciers and ice sheets, permafrost, and karst and karstic systems as a supplementary information on potential uncertainties in hydrologic model process representation and subsurface parameter estimation. The same map layers are also plotted in Figs. 3, 4a, and 4b on top of Sr and WTD. Data sources: ESA Permafrost CCI (processed), GLIMS glacier database (aggregated), WOKAM karst and karstic systems map.

equilibrium conditions, which quickly becomes computationally prohibitive at scale. In fact, any changes in hydraulic properties, boundary conditions, or forcings necessitate a new spinup, which also holds in case of calibration and data assimilation Ultimately, AI technologies are a promising alternative to physics-based simulation (Bennett et al., 2024) to achieve an approximate spinup fast (Ajami et al., 2014), which can be used as an initial condition for further fine tuning. However, in case of applied prediction tasks, training AI on simulation results based on simplified and uncertain hydrogeologic heterogeneity representations limits their utility.

Currently, exascale HPC environments become more common place. In natural science, to fully grasp the potential of these resources is difficult for simulation research. For example, loading one tenth of the new and upcoming JUPITER modular exascale machine (Herten et al., 2024) with the current configuration of the global model would allow a lateral spatial resolution of 100 m. These types of resources open entirely new avenues of research also with respect to uncertainty quantification, which have been unthinkable before.

In the context of the presented proof-of-concept study and future exascale applications, the big data analytics challenge is obvious. Common I/O is not feasible during runtime and also in postprocessing and analyzing the results. For example, the current configuration results in output of, e.g., 3D pressure head distribution in single or double precision without compression on the order of 10^1 GB for a single time step. Going toward science cases at the exascale will result in single file sizes of 10^3 GB, which is not tractable. Thus, in-situ technologies, working on the data during the simulations at run-time are essential (Childs et al., 2019; Do et al., 2022).

The technologies needed to address these technical challenges already exist and are widely used in other scientific and industrial fields. In hydrogeology and groundwater modeling, the community must keep pace with the rapid advancements in these technologies. Challenging questions about the past, present, and future state of the terrestrial water continuum on a global scale—where insights can be learned, generalized, and transferred across regions—may serve as the catalyst needed to drive technological and scientific progress within our field.

3. Methods

3.1. ParFlow model

ParFlow is a 3D variably saturated groundwater surface water flow model, which also integrates the land surface model CLM (not applied in this study). For variably saturated groundwater flow, Richards equation has been implemented based on finite differences. The overland flow boundary condition has been implemented using finite volumes with options for kinematic or diffusive waves. In the second step of the spinup, when lateral routing is activated, the kinematic wave approximation is used in the simulations.

The model was constructed with a resolution $\Delta x = \Delta y = 1km$. Because ParFlow currently still works on a structured grid in Cartesian corrdinates, the error in the cell areas increases from the equator to the poles. The vertical discretization Δz increases vertically from 0.02 to 18 m across 15 layers resulting in a total depth of the subsurface compartment of 60 m. In the current model setup, this depth is constant globally and chosen rather arbitrary to focus on shallow aquifer systems connected to the land surface relevant in ESM at time scales up to decades. In future, variable depth will be implemented based on more detailed hydrogeologic and depth-to-bedrock information.

3.2. Hydrofacies and indicator distribution

The procedure to build the indicator file largely follows the methodology proposed by Belleflamme et al. (2023). For the upper soil characteristics, above the depth-to-bedrock, we use the soil texture (sand, silt, and clay fraction) from the global dataset SoilGrids250m v2017 (Hengl et al., 2017). The data is first bilinearly regridded to our regular lat/lon grid. Then, the seven SoilGrids layers, which cover the upper 2 m, are linearly interpolated to match the depth layers of our grid. Between 2 m depth and the depth-to-bedrock, the soil texture is considered constant. After the interpolation, the texture fractions are rescaled to sum up to 100 % at each grid point. Missing data are interpolated with the nearest neighbor method. Then, the soil texture is classified into the 12 USDA texture classes, so that the soil hydraulic properties from the Rosetta framework (Zhang and Schaap, 2017) can be assigned to each grid point. The depth-to-bedrock is also taken from SoilGrids250m v2017 and bilinearly interpolated in the same way as the soil texture. Below the depth-to-bedrock, we have rasterized the

geometries of the nine geological types from the GLHYMPS dataset (Global HYdrogeology MaPS, Gleeson et al., 2014) to our regular grid, using the nearest neighbor method. The lowest layer is defined to have the GLHYMPS types everywhere. Seas and oceans are masked out as a separate type using the land-sea mask.

3.3. Effective recharge fields

We applied potential recharge (precipitation minus evapotranspiration) as a forcing across the top layer of our modeling setup to achieve a steady-state configuration. Effective recharge, R_{eff}, was calculated using ISIMIP2b global water outputs, which are based on simulations from global water models following the ISIMIP2b protocol (Gosling et al., 2025). Specifically, we used precipitation and actual evapotranspiration values from the CLM4.5 model (Lawrence et al., 2011) at a 0.5° resolution. Monthly average R_{eff} was first calculated using multi-year monthly data from 1861 to 2005. These multi-year monthly averages were then used to calculate and effective yearly R_{eff} and interpolated using the first-order conservative interpolation method (Jones, 1999) to match our model grid at 1 km resolution.

3.4. Topographic slopes

In ParFlow the topographic slopes represent the orography and thus determine the shape of the terrain following grid and the overland flow routing, which leads to the development of the river network. Slopes are defined such that there is a D4 flow direction per grid cell; the flow is directed either towards the North, South, East, or West. The slopes are calculated based on the ASTER global digital elevation model (GDEM) (Abrams et al., 2020). The preprocessing avoids local depressions that would lead to unrealistic surface water ponding heights. In order to ensure a terrain-determined realistic river network (in ParFlow the water flows towards the convergence zones, i.e., river valleys, through gravity or overland flow), the hydrologically adjusted MERIT GDEM (Yamazaki et al., 2019) is used to correct the direction of the slopes wherever needed to ensure each grid cell is drained.

3.5. Boundary conditions

The treatment of the lateral boundary conditions and, in this context, the oceans requires special discussion. In our global setup, the oceans are part of the computational domain with some default hydraulic parameter values assigned to ocean grid cells constituting a brute-force approach. While this appears to be inefficient, and indeed is to a certain degree, the approach bears a major advantage. While coastlines and continental shelf regions are not realistically represented in the model in general, by including the oceans in the computational domain, we do not need to define arbitrary boundary conditions along the continental margins. Thus, groundwater head and fluxes are allowed to dynamically adjust. Arbitrary boundary conditions (in our case no-flow) applied around the rectangular global domain do not influence the solution on the continents. The major disadvantage is that each iterative solution includes ocean grid cells, increasing the condition number of the pressure matrix, compute and storage. Preconditioning, accelerator computing and postprocessing mitigate these disadvantages to a large degree. For completeness, the lower boundary condition at a depth of 60 m was arbitrarily defined as no-flow. Interactions with deeper aquifers and flow paths can not be accounted for in the current implementation.

3.6. Glacier, ice sheet, karst and karstic systems map

The construction of the 3D hydrofacies distribution in the ParFlow IHM is based on SoilGrids v2017 (Hengl et al., 2017) and below the depth-to-bedrock variable of SoilGrids soil hydraulic are used from the Gleeson et al. (2014) GLHYMPS subsurface dataset based on global lithology maps. In addition to Fig. 1, which exemplifies the ParFlow hydrofacies distribution from the GLHYMPS dataset, Fig. 5 contains areas of the global ParFlow model domain that are either difficult to simulate due to process representation, such as permafrost soils (Obu, 2021) and glaciated regions (mountain glaciers and ice sheets), and/or where a complex hydrogeological situation due to karst or karstic systems rock formations (Chen et al., 2017) may lead to or is associated with a lithology with high and highly heterogeneous permeabilities and hydraulic conductivities that are difficult to account for in the static subsurface parameters of any model system. The additional state-of-the-art data for glaciers and ice sheets has been derived and generalized from the Global Land Ice Measurements from Space glacier database (GLIMS) (GLIMS and NSIDC, 2005, updated 2018). The continuous and discontinuous permafrost is a spatially aggregated long-term mean (1997 to 2023) binary mask based on the ESA Permafrost Climate Change Initiative dataset permafrost fraction per area (Westermann et al., 2025). The karst and karstic systems overview in Fig. 5 is from the World Karst Aquifer Map (WOKAM) (Chen et al., 2017). Note that these map layers are also plotted onto Fig. 3, and Fig. 4a and 4b to indicate simulation results, which may be considered less reliable.

Declaration of competing interest

The authors declare that they have no known competing financial interests or personal relationships that could have appeared to influence the work reported in this paper.

Acknowledgements

The authors gratefully acknowledge the Earth System Modelling Project (ESM) for funding this work by providing computing time on the ESM partition of the supercomputer JUWELS (Alvarez, 2021) at the Jülich Supercomputing Centre (JSC). The study on which this article is based was partially funded by the German Federal Ministry of Education and Research under the funding code 01LK2202 in the WarmWorld project. The responsibility for the content of this publication lies with the authors. This project has received funding also from the European High Performance Computing Joint Undertaking under grant agreement n°101144014. Views and opinions expressed are however those of the author(s) only and do not necessarily reflect those of the European Union or the EuroHPC JU. Neither the European Union nor the granting authority can be held responsible for them.

CRediT authorship contribution statement

SK designed the proof-of-concept study, implemented the model, performed the simulations, analyzed the results and wrote the manuscript. AB generated model input data, discussed the results and revised and wrote parts of the manuscript. LC discussed the results and revised and wrote parts of the manuscript. MF contributed high-performance computing developments, and performance monitoring and tuning for efficient performance of the simulations. KG generated the plots, discussed the results and revised and wrote parts of the manuscript. RM discussed the results and revised and wrote parts of the manuscript. BN generated model input data, discussed the results and revised and wrote parts of the manuscript.

Data availability

Data will be made available on request.

References

Abrams, M., Crippen, R., Fujisada, H., 2020. ASTER global digital elevation model (GDEM) and ASTER global water body dataset (ASTWBD). Remote Sens. (Basel) 12. https://doi.org/10.3390/rs12071156.

Adams, K.H., Reager, J.T., Rosen, P., Wiese, D.N., Farr, T.G., Rao, S., Haines, B.J., Argus, D.F., Liu, Z., Smith, R., Famiglietti, J.S., Rodell, M., 2022. Remote sensing of

groundwater: current capabilities and future directions. Water Resour. Res. 58, e2022WR032219. https://doi.org/10.1029/2022WR032219.
Ajami, H., Evans, J.P., McCabe, M.F., Stisen, S., 2014. Technical note: reducing the spin-up time of integrated surface water–groundwater models. Hydrol. Earth Syst. Sci. 18, 5169–5179. https://doi.org/10.5194/hess-18-5169-2014.
Alvarez, D., 2021. JUWELS cluster and booster: exascale pathfinder with modular supercomputing architecture at juelich supercomputing centre. Journal of Large-Scale Research Facilities JLSRF 7, A183. https://doi.org/10.17815/jlsrf-7-183.
Anderson, M.P., 1989. Hydrogeologic facies models to delineate large-scale spatial trends in glacial and glaciofluvial sediments. Geol. Soc. Am. Bull. 101, 501–511. https://doi.org/10.1130/0016-7606(1989)101<0501:HFMTDL>2.3.CO;2.
Andréassian, V., 2023. On the (im)possible validation of hydrogeological models. Comptes Rendus. Géoscience 355, 337–345. https://doi.org/10.5802/crgeos.142.
Bauer, P., Dueben, P.D., Hoefler, T., Quintino, T., Schulthess, T.C., Wedi, N.P., 2021. The digital revolution of earth-system science. Nat. Comput. Sci. 1, 104–113. https://doi.org/10.1038/s43588-021-00023-0.
Belleflamme, A., Goergen, K., Wagner, N., Kollet, S., Bathiany, S., El Zohbi, J., Rechid, D., Vanderborght, J., Vereecken, H., 2023. Hydrological forecasting at impact scale: the integrated ParFlow hydrological model at 0.6 km for climate resilient water resource management over Germany. Front. Water 5, 1183642. https://doi.org/10.3389/frwa.2023.1183642.
Bennett, A., Tran, H., De La Fuente, L., Triplett, A., Ma, Y., Melchior, P., Maxwell, R.M., Condon, L.E., 2024. Spatio-temporal machine learning for regional to continental scale terrestrial hydrology. J. Adv. Model. Earth Syst. 16, e2023MS004095. https://doi.org/10.1029/2023MS004095.
Bierkens, M.F.P., Bell, V.A., Burek, P., Chaney, N., Condon, L.E., David, C.H., de Roo, A., Döll, P., Drost, N., Famiglietti, J., 2015. Hyper-resolution global hydrological modelling: what is next? Hydrol. Process. 29, 310–320. https://doi.org/10.1002/hyp.10391.
Brookfield, A.E., Ajami, H., Carroll, R.W.H., Tague, C., Sullivan, P.L., Condon, L.E., 2023. Recent advances in integrated hydrologic models: Integration of new domains. J. Hydrol. 620, 129515. https://doi.org/10.1016/j.jhydrol.2023.129515.
Burstedde, C., Fonseca, J.A., Kollet, S., 2018. Enhancing speed and scalability of the ParFlow simulation code. Comput. Geosci. 22, 347–361. https://doi.org/10.1007/s10596-017-9696-2.
Chen, Z., Goldscheider, N., Auler, A., Bakalowicz, M., Broda, S., Drew, D., Hartmann, J., Jiang, G., Moosdorf, N., Richts, A., Stevanovic, Z., Veni, G., Dumont, A., Aureli, A., Clos, P., Krombholz, M., 2017. World Karst Aquifer Map (WHYMAP WOKAM). BGR, IAH, KIT, UNESCO. Doi: 10.25928/b2.21_sfkq-r406.
Childs, H., Janine Bennett, J., Garth, C., Hentschel, B., 2019. In situ visualization for computational science. IEEE Comput. Graph. Appl. 39. https://doi.org/10.1109/mcg.2019.2936674.
Clark, M.P., Bierkens, M.F.P., Samaniego, L., Woods, R.A., Uijlenhoet, R., Bennett, K.E., Pauwels, V.R.N., Cai, X., Wood, A.W., Peters-Lidard, C.D., 2017. The evolution of process-based hydrologic models: Historical challenges and the collective quest for physical realism. Hydrol. Earth Syst. Sci. 21, 3427–3440. https://doi.org/10.5194/hess-21-3427-2017.
Clark, M.P., Nijssen, B., Lundquist, J.D., Kavetski, D., Rupp, D.E., Woods, R.A., Freer, J. E., Gutmann, E.D., Wood, A.W., Gochis, D.J., Rasmussen, R.M., Tarboton, D.G., Mahat, V., Flerchinger, G.N., Marks, D.G., 2015. A unified approach for process-based hydrologic modeling: 2. Model implementation and case studies. Water Resour. Res. 51, 2515–2542. https://doi.org/10.1002/2015WR017200.
Condon, L.E., Kollet, S., Bierkens, M.F.P., Fogg, G.E., Maxwell, R.M., Hill, M.C., Fransen, H.H., Verhoef, A., Van Loon, A.F., Sulis, M., Abesser, C., 2021. Global groundwater modeling and monitoring: opportunities and challenges. Water Resour. Res. 57, e2020WR029500. https://doi.org/10.1029/2020WR029500.
De Graaf, I.E.M., Gleeson, T., (Rens) Van Beek, L.P.H., Sutanudjaja, E.H., Bierkens, M.F. P., 2019. Environmental flow limits to global groundwater pumping. Nature 574, 90–94. https://doi.org/10.1038/s41586-019-1594-4.
De Graaf, I.E.M., Sutanudjaja, E.H., Van Beek, L.P.H., Bierkens, M.F.P., 2015. A high-resolution global-scale groundwater model. Hydrol. Earth Syst. Sci. 19, 823–837. https://doi.org/10.5194/hess-19-823-2015.
Do, T.M.A., Pottier, L., Yildiz, O., Vahi, K., Krawczuk, P., Peterka, T., Deelman, E., 2022. Accelerating scientific workflows on HPC platforms with in situ processing. In: 2022 22nd IEEE International Symposium on Cluster, Cloud and Internet Computing (CCGrid), pp. 1–10. https://doi.org/10.1109/CCGrid54584.2022.00009.
Famiglietti, J.S., 2014. The global groundwater crisis. Nat. Clim. Chang. 4, 945. https://doi.org/10.1038/nclimate2425.
Fan, Y., Clark, M., Lawrence, D.M., Swenson, S., Band, L.E., Brantley, S.L., Brooks, P.D., Dietrich, W.E., Flores, A., Grant, G., Kirchner, J.W., Mackay, D.S., McDonnell, J.J., Milly, P.C.D., Sullivan, P.L., Tague, C., Ajami, H., Chaney, N., Hartmann, A., Hazenberg, P., McNamara, J., Pelletier, J., Perket, J., Rouholahnejad-Freund, E., Wagener, T., Zeng, X., Beighley, E., Buzan, J., Huang, M., Livneh, B., Mohanty, B.P., Nijssen, B., Safeeq, M., Shen, C., Van Verseveld, W., Volk, J., Yamazaki, D., 2019. Hillslope hydrology in global change research and earth system modeling. Water Resour. Res. 55, 1737–1772. https://doi.org/10.1029/2018WR023903.
Fan, Y., Li, H., Miguez-Macho, G., 2013. Global patterns of groundwater table depth. Science 339, 940–943. https://doi.org/10.1126/science.1229881.
Fisher, R.A., Koven, C.D., 2020. Perspectives on the future of land surface models and the challenges of representing complex terrestrial systems. J. Adv. Model. Earth Syst. 12, e2018MS001453. https://doi.org/10.1029/2018MS001453.
Furusho-Percot, C., Goergen, K., Hartick, C., Kulkarni, K., Keune, J., Kollet, S., 2019. Pan-European groundwater to atmosphere terrestrial systems climatology from a physically consistent simulation. Sci. Data 6, 320. https://doi.org/10.1038/s41597-019-0328-7.
Gleeson, T., Moosdorf, N., Hartmann, J., van Beek, L.P.H., 2014. A glimpse beneath earth's surface: GLobal HYdrogeology MaPS (GLHYMPS) of permeability and porosity. Geophys. Res. Lett. 41 (11), 3891–3898. https://doi.org/10.1002/2014GL059856.
Gleeson, T., Wagener, T., Döll, P., Zipper, S.C., West, C., Wada, Y., Taylor, R., Scanlon, B., Rosolem, R., Rahman, S., Oshinlaja, N., Maxwell, R., Lo, M.-H., Kim, H., Hill, M., Hartmann, A., Fogg, G., Famiglietti, J.S., Ducharne, A., de Graaf, I., Cuthbert, M., Condon, L., Bresciani, E., Bierkens, M.F.P., 2021. GMD perspective: the quest to improve the evaluation of groundwater representation in continental- to global-scale models. Geosci. Model Dev. 14, 7545–7571. https://doi.org/10.5194/gmd-14-7545-2021.
GLIMS and NSIDC, 2005, updated 2018. Global Land Ice Measurements from Space glacier database. Compiled and made available by the international GLIMS community and the National Snow and Ice Data Center, Boulder CO, U.S.A. Doi: 10.7265/N5V98602.
Gnann, S., Reinecke, R., Stein, L., Wada, Y., Thiery, W., Müller Schmied, H., Satoh, Y., Pokhrel, Y., Ostberg, S., Koutroulis, A., Hanasaki, N., Grillakis, M., Gosling, S.N., Burek, P., Bierkens, M.F.P., Wagener, T., 2023. Functional relationships reveal differences in the water cycle representation of global water models. Nat. Water 1, 1079–1090. https://doi.org/10.1038/s44221-023-00160-y.
Gosling, S.N., Burek, P., Chang, J., Ciais, P., Döll, P., et al. 2025. ISIMIP2b Simulation Data from the GLobal Water Sector (v1.1). ISIMIP Repository. https://doi.org/10.48364/ISIMIP.626689.1.
Hengl, T., Mendes de Jesus, J., Heuvelink, G.B.M., Ruiperez Gonzalez, M., Kilibarda, M., Blagotić, A., et al., 2017. SoilGrids250m: global gridded soil information based on machine learning. PLoS One 12 (2), 1–40. https://doi.org/10.1371/journal.pone.0169748.
Herten, A., Achilles, S., Alvarez, D., Badwaik, J., Behle, E., Bode, M., Breuer, T., Caviedes-Voullième, D., Cherti, M., Dabah, A., Sayed, S.E., Frings, W., Gonzalez-Nicolas, A., Gregory, E.B., Mood, K.H., Hater, T., Jitsev, J., John, C.M., Meinke, J.H., Meyer, C.I., Mezentsev, P., Mirus, J.-O., Nassyr, S., Penke, C., Römmer, M., Sinha, U., Vieth, B. von St., Stein, O., Suarez, E., Willsch, D., Zhukov, I., 2024. Application-driven exascale: The JUPITER benchmark suite, in: SC24: International Conference for High Performance Computing, Networking, Storage and Analysis. pp. 1–45. Doi: 10.1109/SC41406.2024.00038.
Hokkanen, J., Kollet, S., Kraus, J., Herten, A., Hrywniak, M., Pleiter, D., 2021. Leveraging HPC accelerator architectures with modern techniques — hydrologic modeling on GPUs with ParFlow. Comput. Geosci. 25, 1579–1590. https://doi.org/10.1007/s10596-021-10051-4.
Hydrologic unit maps, 1987. Doi: 10.3133/wsp2294.
Ibrahim, A., Wayayok, A., Shafri, H.Z.M., Toridi, N.M., 2024. Remote sensing technologies for unlocking new groundwater insights: a comprehensive review. J. Hydrol. X 23, 100175. https://doi.org/10.1016/j.hydroa.2024.100175.
Jasechko, S., Seybold, H., Perrone, D., Fan, Y., Shamsudduha, M., Taylor, R.G., Fallatah, O., Kirchner, J.W., 2024. Rapid groundwater decline and some cases of recovery in aquifers globally. Nature 625, 715–721. https://doi.org/10.1038/s41586-023-06879-8.
Jones, P.W., 1999. First- and second-order conservative remapping schemes for grids in spherical coordinates. Mon. Wea. Rev. 127, 2204–2210. https://doi.org/10.1175/1520-0493(1999)127<2204:FASOCR>2.0.CO;2.
Jones, J.E., Woodward, C.S., 2001. Newton–Krylov-multigrid solvers for large-scale, highly heterogeneous, variably saturated flow problems. Adv. Water Resour. 24, 763–774. https://doi.org/10.1016/S0309-1708(00)00075-0.
Kavetski, D., Clark, M.P., 2011. Numerical troubles in conceptual hydrology: approximations, absurdities and impact on hypothesis testing. Hydrol. Process. 25, 661–670. https://doi.org/10.1002/hyp.7899.
Keune, J., Sulis, M., Kollet, S., Siebert, S., Wada, Y., 2018. Human water use impacts on the strength of the continental sink for atmospheric water. Geophys. Res. Lett. 45, 4068–4076. https://doi.org/10.1029/2018GL077621.
Klingbeil, R., Kleineidam, S., Asprion, U., Aigner, T., Teutsch, G., 1999. Relating lithofacies to hydrofacies: outcrop-based hydrogeological characterisation of quaternary gravel deposits. Sed. Geol. 129, 299–310. https://doi.org/10.1016/S0037-0738(99)00067-6.
Knijff, J.M.V.D., Younis, J., and, A.P.J.D.R., 2010. LISFLOOD: A GIS-based distributed model for river basin scale water balance and flood simulation. Int. J. Geogr. Inform. Sci., 24, 189–212. Doi: 10.1080/13658810802549154.
Kollet, S.J., Maxwell, R.M., 2006. Integrated surface–groundwater flow modeling: a free-surface overland flow boundary condition in a parallel groundwater flow model. Adv. Water Resour. 29, 945–958. https://doi.org/10.1016/j.advwatres.2005.08.006.
Kollet, S., Sulis, M., Maxwell, R.M., Paniconi, C., Putti, M., Bertoldi, G., Coon, E.T., Cordano, E., Endrizzi, S., Kikinzon, E., Mouche, E., Mügler, C., Park, Y.-J., Refsgaard, J.C., Stisen, S., Sudicky, E., 2017. The integrated hydrologic model intercomparison project, IH-MIP2 : a second set of benchmark results to diagnose integrated hydrology and feedback. Water Resour. Res. 53, 867–890. https://doi.org/10.1002/2016WR019191.
Krinner, G., Viovy, N., de Noblet-Ducoudré, N., Ogée, J., Polcher, J., Friedlingstein, P., Ciais, P., Sitch, S., Prentice, I.C., 2005. A dynamic global vegetation model for studies of the coupled atmosphere-biosphere system. Global Biogeochem. Cycles 19. https://doi.org/10.1029/2003GB002199.
Kuffour, B.N.O., Engdahl, N.B., Woodward, C.S., Condon, L.E., Kollet, S., Maxwell, R.M., 2020. Simulating coupled surface–subsurface flows with ParFlow v3.5.0: capabilities, applications, and ongoing development of an open-source, massively parallel, integrated hydrologic model. Geosci. Model Dev. 13, 1373–1397. https://doi.org/10.5194/gmd-13-1373-2020.

Lawrence, D.M., Oleson, K.W., Flanner, M.G., Thornton, P.E., Swenson, S.C., Lawrence, P.J., 2011. Parametrization improvements and functional and structural advances in Version 4 of the Community Land Model. J. Adv. Model. Earth Syst. 3, M03001. https://doi.org/10.1029/2011MS00045.

Lawrence, D.M., Fisher, R.A., Koven, C.D., Oleson, K.W., Swenson, S.C., Bonan, G., Collier, N., Ghimire, B., van Kampenhout, L., Kennedy, D., Kluzek, E., Lawrence, P.J., Li, F., Li, H., Lombardozzi, D., Riley, W.J., Sacks, W.J., Shi, M., Vertenstein, M., Wieder, W.R., Xu, C., Ali, A.A., Badger, A.M., Bisht, G., van den Broeke, M., Brunke, M.A., Burns, S.P., Buzan, J., Clark, M., Craig, A., Dahlin, K., Drewniak, B., Fisher, J.B., Flanner, M., Fox, A.M., Gentine, P., Hoffman, F., Keppel-Aleks, G., Knox, R., Kumar, S., Lenaerts, J., Leung, L.R., Lipscomb, W.H., Lu, Y., Pandey, A., Pelletier, J.D., Perket, J., Randerson, J.T., Ricciuto, D.M., Sanderson, B.M., Slater, A., Subin, Z.M., Tang, J., Thomas, R.Q., Val Martin, M., Zeng, X., 2019. The community land model version 5: description of new features, benchmarking, and impact of forcing uncertainty. J. Adv. Model. Earth Syst. 11, 4245–4287. https://doi.org/10.1029/2018MS001583.

Lindström, G., Johansson, B., Persson, M., Gardelin, M., Bergström, S., 1997. Development and test of the distributed HBV-96 hydrological model. J. Hydrol. 201, 272–288. https://doi.org/10.1016/S0022-1694(97)00041-3.

Maxwell, R.M., 2013. A terrain-following grid transform and preconditioner for parallel, large-scale, integrated hydrologic modeling. Adv. Water Resour. 53, 109–117. https://doi.org/10.1016/j.advwatres.2012.10.001.

Maxwell, R.M., Putti, M., Meyerhoff, S., Delfs, J.-O., Ferguson, I.M., Ivanov, V., Kim, J., Kolditz, O., Kollet, S.J., Kumar, M., Lopez, S., Niu, J., Paniconi, C., Park, Y.-J., Phanikumar, M.S., Shen, C., Sudicky, E.A., Sulis, M., 2014. Surface-subsurface model intercomparison: a first set of benchmark results to diagnose integrated hydrology and feedbacks. Water Resour. Res. 50, 1531–1549. https://doi.org/10.1002/2013WR013725.

Müller Schmied, H., Cáceres, D., Eisner, S., Flörke, M., Herbert, C., Niemann, C., Peiris, T. A., Popat, E., Portmann, F.T., Reinecke, R., Schumacher, M., Shadkam, S., Telteu, C.-E., Trautmann, T., Döll, P., 2021. The global water resources and use model WaterGAP v2.2d: model description and evaluation. Geosci. Model Dev. 14, 1037–1079. https://doi.org/10.5194/gmd-14-1037-2021.

Niu, G.-Y., Yang, Z.-L., Mitchell, K.E., Chen, F., Ek, M.B., Barlage, M., Kumar, A., Manning, K., Niyogi, D., Rosero, E., Tewari, M., Xia, Y., 2011. The community noah land surface model with multiparameterization options (noah-MP): 1. Model description and evaluation with local-scale measurements. J. Geophys. Res. Atmos. 116. https://doi.org/10.1029/2010JD015139.

Obu, J., 2021. How much of the earth's surface is underlain by permafrost? J. Geophys. Res. Earth 126 (5), e2021JF006123. https://doi.org/10.1029/2021JF006123.

Pan, X., Chen, D., Pan, B., Huang, X., Yang, K., Piao, S., Zhou, T., Dai, Y., Chen, F., Li, X., 2025. Evolution and prospects of earth system models: challenges and opportunities. Earth Sci. Rev. 260, 104986. https://doi.org/10.1016/j.earscirev.2024.104986.

Poshyvailo-Strube, L., Wagner, N., Goergen, K., Furusho-Percot, C., Hartick, C., Kollet, S., 2024. Impact of groundwater representation on heat events in regional climate simulations over Europe. Earth Syst. Dyn. 15, 167–189. https://doi.org/10.5194/esd-15-167-2024.

Prein, A.F., Langhans, W., Fosser, G., Ferrone, A., Ban, N., Goergen, K., Keller, M., Tölle, M., Gutjahr, O., Feser, F., Brisson, E., Kollet, S., Schmidli, J., Van Lipzig, N.P. M., Leung, R., 2015. A review on regional convection-permitting climate modeling: demonstrations, prospects, and challenges. Rev. Geophys. 53, 323–361. https://doi.org/10.1002/2014RG000475.

Reinecke, R., Foglia, L., Mehl, S., Trautmann, T., Cáceres, D., Döll, P., 2019. Challenges in developing a global gradient-based groundwater model (G^3 M v1.0) for the integration into a global hydrological model. Geosci. Model Dev. 12, 2401–2418. https://doi.org/10.5194/gmd-12-2401-2019.

Reinecke, R., Gnann, S., Stein, L., Bierkens, M., De Graaf, I., Gleeson, T., Essink, G.O., Sutanudjaja, E.H., Ruz Vargas, C., Verkaik, J., Wagener, T., 2024. Uncertainty in model estimates of global groundwater depth. Environ. Res. Lett. 19, 114066. https://doi.org/10.1088/1748-9326/ad8587.

Samaniego, L., Kumar, R., Attinger, S., 2010. Multiscale parameter regionalization of a grid-based hydrologic model at the mesoscale. Water Resour. Res. 46. https://doi.org/10.1029/2008WR007327.

Sophocleous, M., 2002. Interactions between groundwater and surface water: the state of the science. Hydrgeol. J. 10, 52–67. https://doi.org/10.1007/s10040-001-0170-8.

Stevens, B., Adami, S., Ali, T., Anzt, H., Aslan, Z., Attinger, S., Bäck, J., Baehr, J., Bauer, P., Bernier, N., Bishop, B., Bockelmann, H., Bony, S., Brasseur, G., Bresch, D. N., Breyer, S., Brunet, G., Buttigieg, P.L., Cao, J., Castet, C., Cheng, Y., Dey Choudhury, A., Coen, D., Crewell, S., Dabholkar, A., Dai, Q., Doblas-Reyes, F., Durran, D., El Gaidi, A., Ewen, C., Exarchou, E., Eyring, V., Falkinhoff, F., Farrell, D., Forster, P.M., Frassoni, A., Frauen, C., Fuhrer, O., Gani, S., Gerber, E., Goldfarb, D., Grieger, J., Gruber, N., Hazeleger, W., Herken, R., Hewitt, C., Hoefler, T., Hsu, H.-H., Jacob, D., Jahn, A., Jakob, C., Jung, T., Kadow, C., Kang, I.-S., Kang, S., Kashinath, K., Kleinen-von Königslöw, K., Klocke, D., Kloenne, U., Klöwer, M., Kodama, C., Kollet, S., Kölling, T., Kontkanen, J., Kopp, S., Koran, M., Kulmala, M., Lappalainen, H., Latifi, F., Lawrence, B., Lee, J.Y., Lejeun, Q., Lessig, C., Li, C., Lippert, T., Luterbacher, J., Manninen, P., Marotzke, J., Matsouoka, S., Merchant, C., Messmer, P., Michel, G., Michielsen, K., Miyakawa, T., Müller, J., Munir, R., Narayanasetti, S., Ndiaye, O., Nobre, C., Oberg, A., Oki, R., Özkan-Haller, T., Palmer, T., Posey, S., Prein, A., Primus, O., Pritchard, M., Pullen, J., Putrasahan, D., Quaas, J., Raghavan, K., Ramaswamy, V., Rapp, M., Rauser, F., Reichstein, M., Revi, A., Saluja, S., Satoh, M., Schemann, V., Schemm, S., Schnadt Poberaj, C., Schulthess, T., Senior, C., Shukla, J., Singh, M., Slingo, J., Sobel, A., Solman, S., Spitzer, J., Stier, P., Stocker, T., Strock, S., Su, H., Taalas, P., Taylor, J., Tegtmeier, S., Teutsch, G., Tompkins, A., Ulbrich, U., Vidale, P.-L., Wu, C.-M., Xu, H., Zaki, N., Zanna, L., Zhou, T., Ziemen, F., 2024. Earth virtualization engines (EVE). Earth Syst. Sci. Data 16, 2113–2122. https://doi.org/10.5194/essd-16-2113-2024.

Sutanudjaja, E.H., van Beek, R., Wanders, N., Wada, Y., Bosmans, J.H.C., Drost, N., van der Ent, R.J., de Graaf, I.E.M., Hoch, J.M., de Jong, K., Karssenberg, D., López López, P., Peßenteiner, S., Schmitz, O., Straatsma, M.W., Vannametee, E., Wisser, D., Bierkens, M.F.P., 2018. PCR-GLOBWB 2: a 5 arcmin global hydrological and water resources model. Geosci. Model Dev. 11, 2429–2453. https://doi.org/10.5194/gmd-11-2429-2018.

Telteu, C.-E., Müller Schmied, H., Thiery, W., Leng, G., Burek, P., Liu, X., Boulange, J.E. S., Andersen, L.S., Grillakis, M., Gosling, S.N., Satoh, Y., Rakovec, O., Stacke, T., Chang, J., Wanders, N., Shah, H.L., Trautmann, T., Mao, G., Hanasaki, N., Koutroulis, A., Pokhrel, Y., Samaniego, L., Wada, Y., Mishra, V., Liu, J., Döll, P., Zhao, F., Gädeke, A., Rabin, S.S., Herz, F., 2021. Understanding each other's models: an introduction and a standard representation of 16 global water models to support intercomparison, improvement, and communication. Geosci. Model Dev. 14, 3843–3878. https://doi.org/10.5194/gmd-14-3843-2021.

Tijerina-Kreuzer, D., Swilley, J.S., Tran, H.V., Zhang, J., West, B., Yang, C., Condon, L.E., Maxwell, R.M., 2024. Continental scale hydrostratigraphy: basin-scale testing of alternative data-driven approaches. Groundwater 62, 93–110. https://doi.org/10.1111/gwat.13357.

Verkaik, J., Sutanudjaja, E.H., Oude Essink, G.H.P., Lin, H.X., Bierkens, M.F.P., 2024. GLOBGM v1.0: a parallel implementation of a 30 arcsec PCR-GLOBWB-MODFLOW global-scale groundwater model. Geosci. Model Dev. 17, 275–300. https://doi.org/10.5194/gmd-17-275-2024.

Westermann, S., Barboux, C., Bartsch, A., Delaloye, R., Grosse, G., Heim, B., Hugelius, G., Irrgang, A., Kääb, A.M., Matthes, H., Miesner, F., Nitze, I., Pellet, C., Seifert, F.M., Strozzi, T., Wegmüller, U., Wieczorek, M., Wiesmann, A., 2025: ESA permafrost climate change initiative (Permafrost_cci): permafrost extent for the northern hemisphere, v5.0. NERC EDS Centre for Environmental Data Analysis, 28 August 2025. Doi: 10.5285/d235665772ec4b558e9a89ac85595e71.

Wood, E.F., Roundy, J.K., Troy, T.J., van Beek, L.P.H., Bierkens, M.F.P., Blyth, E., de Roo, A., Döll, P., Ek, M., Famiglietti, J., 2011. Hyperresolution global land surface modeling: meeting a grand challenge for monitoring earth's terrestrial water. Water Resour. Res. 47. https://doi.org/10.1029/2010WR010090.

Yamazaki, D., Ikeshima, D., Sosa, J., Bates, P.D., Allen, G.H., Pavelsky, T.M., 2019. MERIT hydro: a high-resolution global hydrography map based on latest topography dataset. Water Resour. Res. 55, 5053–5073. https://doi.org/10.1029/2019WR024873.

Yang, C., Condon, L.E., Maxwell, R.M., 2025. Unravelling groundwater–stream connections over the continental United States. Nat. Water 3, 70–79. https://doi.org/10.1038/s44221-024-00366-8.

Yang, C., Tijerina-Kreuzer, D.T., Tran, H.V., Condon, L.E., Maxwell, R.M., 2023. A high-resolution, 3D groundwater-surface water simulation of the contiguous US: advances in the integrated ParFlow CONUS 2.0 modeling platform. J. Hydrol. 626, 130294. https://doi.org/10.1016/j.jhydrol.2023.130294.

Zhang, Y., Schaap, M.G., 2017. Weighted recalibration of the Rosetta pedotransfer model wih improved estimates of hydraulic parameter distributions and summary statistics (Rosetta3). J. Hydrol. 547, 39–53. https://doi.org/10.1016/j.jhydrol.2017.01.004.